THE ASTROPHYSICAL JOURNAL, 426:192–203, 1994 May 1

ON THE VELOCITY DISPERSION IN THE CORE OF THE GLOBULAR CLUSTER M15[1]

P. DUBATH AND G. MEYLAN
European Southern Observatory, Karl-Schwarzschild-Strasse 2, D-85748 Garching bei München, Germany
E-mail: pdubath@eso.org; meylan@eso.org

AND

M. MAYOR
Geneva Observatory, 51, Ch.des Maillettes, CH-1290 Sauverny, Switzerland
E-mail: mayor@scsun.unige.ch

Received 1992 June 19; accepted 1993 November 4

ABSTRACT

A projected velocity dispersion $\sigma_p(0) = 14.0$ km s^{-1} is derived from an integrated light spectrum obtained at the European Southern Observatory (ESO) at La Silla, Chile, over a central $6'' \times 6''$ area in the core of the globular cluster M15. Extensive numerical simulations of velocity dispersion determinations from integrated light spectra show that all the velocity dispersions obtained from integrated light measurements over small central areas suffer from large statistical errors due to the small numbers of bright stars present in the integration area. These simulations, over our area of integration of $6'' \times 6''$, give $\sigma_p = 15^{+6}_{-4}$ km s^{-1} as the most probable values for the central velocity dispersion and its statistical error.

The observational result differs from the challenging high central velocity dispersion $\sigma_p(0) = 25$ km s^{-1} derived by Peterson, Seitzer, & Cudworth (1989) from integrated light spectra over an integration area of about $1'' \times 1''$. Because of our larger sampling area, we would probably miss any central cusp in velocity dispersion. However, our simulations show that the statistical errors, due to small samples, are so large that the results of Peterson et al. (1989) are consistent with ours. In a similar way, all the above velocity dispersion values obtained from integrated light measurements are consistent with the velocity dispersion $\sigma_p = 14.2 \pm 1.9$ km s^{-1} obtained by Peterson et al. (1989) from the radial velocities of 27 stars within 20″ of the center. Given the large statistical errors on the integrated light measurements, there is no significant observational evidence that the central value of the velocity dispersion is much larger than about 15 km s^{-1}. All observed values are consistent with the predictions from various theoretical dynamical models of M15: $\sigma_p(0) = 12$–17 km s^{-1} from Illingworth & King (1977), $\sigma_p(0) = 13$–15 km s^{-1} from Phinney & Sigurdsson (1991) and Phinney (1993), and $\sigma_p(0) = 14$ km s^{-1} from Grabhorn et al. (1992). Although it cannot be ruled out, the presence of a massive black hole or some nonthermal dynamics in the core of M15 is not required by the present observations.

Subject headings: celestial mechanics, stellar dynamics — globular clusters: individual (M15) — ISM: kinematics and dynamics

1. INTRODUCTION

The globular cluster M15 = NGC 7078 has been for a long time the prototype of the collapsed star clusters. Early electrographic determinations of its luminosity profile by Newell & O'Neil (1978), confirmed by further photographic and CCD studies (e.g., Aurière & Cordoni 1981; Hertz & Grindlay 1985; Djorgovski & King 1986), reveal a central excess of light—semi-stellar nucleus about 2″ in radius—superposed on an otherwise usual isothermal core. Newell, Da Costa, & Norris (1976) find these observations consistent with the existence of a central massive object, possibly a black hole of about 800 $M_\odot$, while Illingworth & King (1977) are able, without a black hole, to fit dynamical models successfully to the entire surface-brightness profile. The latter explain the central brightness peak as being caused simply by the gravitational effect of a central population of neutron stars.

In his study of stellar proper motions, Cudworth (1976) gives the first estimate of velocity dispersion in M15, viz. $\sigma_p = 10$–14 km s^{-1} for stars between 1.5 and 12′ from the center. The only other comprehensive work providing observational constraints concerning the dynamics of M15 is published by Peterson, Seitzer, & Cudworth (1989). In their study, the velocity dispersion is derived from two different kinds of data: (1) from individual radial velocities of 120 stars which are members of the cluster, scattered between 0.1 and 4.6 from the center, and (2) from integrated light spectra of the central luminosity cusp. The radial velocities of 27 stars within 20″ of the center give a velocity dispersion $\sigma_p = 14.2 \pm 1.9$ km s^{-1}, while the integrated light spectra suggest a cusp in velocity dispersion, with $\sigma_p(0)$ of at least 25 km s^{-1}. According to this work, the core of M15 would exhibit a sharp rise in velocity dispersion, this within the central few seconds of arc. Peterson et al. (1989) find their cusp in velocity dispersion consistent neither with King-Michie models nor with post-core collapse models. They consider their observations as indications of a nonthermal energy distribution, consistent with a central black hole of about 1000 $M_\odot$.

Since the study of Peterson et al. (1989), high-resolution imaging observations of the core of M15 have resolved the luminosity cusp (although this cusp was already partly resolved in the images published by Aurière, le Fèvre, & Terzan 1984). From the paper by Racine & McClure (1989), using

[1] Based on observations collected at the European Southern Observatory, La Silla, Chile.

HRCam, the High-Resolution Camera of the Canada-France-Hawaii Telescope (CFHT), with FWHM = 0".35, and even more from the paper by Lauer et al. (1991), using the Planetary Camera of the *Hubble Space Telescope* (*HST*), with FWHM = 0".08, it appears that the cusp is easily resolved in a group of a few bright stars (see also Fig. 2 below). The surface-brightness profile of the residual light, obtained after subtracting the bright resolved stars, does not continue to rise at subarcsecond radii, but flattens off interior to a radius of about 2". Laure et al. (1991) determine, from their observations, a core radius of 2".2 = 0.13 pc, and argue that the existence of a core rather than a cusp at the center of M15, may indicate that the central dark matter implied by the high central velocity dispersion estimate of Peterson et al. (1989) does not belong to a massive black hole, but probably resides in a more diffuse form.

Recently, by using their multimass Fokker-Planck model, Grabhorn et al. (1992) fitted successfully their predicted surface-brightness profile, at time of maximal core expansion in the post-collapse phase, to the high-resolution density profile determined by Lauer et al. (1991). Their predicted velocity-dispersion profile matches reasonably well the observations of Peterson et al. (1989), although their preferred model which best fits the observed surface-brightness and velocity-dispersion profiles predicts a central velocity dispersion of 14 km s^{-1}. They also show that a multi-mass King model can fit the observed surface-brightness profile (as well as their multimass Fokker-Planck model), but fail to reproduce the central rise in velocity dispersion. This work emphasizes that it is not necessary to invoke a massive black hole to explain the observations of M15.

As part of a long-term program of determination of central velocity dispersion in the cores of high-concentration and collapsed globular clusters, we obtained, at the European Southern Observatory (ESO) at La Silla, Chile, an integrated light spectrum of the core of M15. Over the last few years, our cross-correlation technique has been applied to a large number of spectra and the derived cross-correlation functions are always extremely well approximated by Gaussian functions. Figure 1 displays, first, the cross-correlation function (CCF) of the spectrum of a standard K0 giant star, HD 203638, second, the CCF of the integrated light spectrum in the core of M15, and third, the CCF of the integrated light spectrum in the core of the galactic globular cluster NGC 362, all three spectra having been obtained under identical conditions (see § 2 below for a complete discussion). The dotted curves represent the CCFs themselves, the continuous lines the fitted Gaussians. The CCFs of the spectra of HD 203638 and of NGC 362 are displayed in order to show how close to a Gaussian the typical CCFs obtained for standard stars and for other galactic globular clusters can be. Totally unexpectedly, and despite the high signal-to-noise ratio of our observed spectrum, the CCF of the M15 spectrum is bumpy, as if it were the sum of two different Gaussians. This large departure from the usual Gaussian function is larger than the deviations produced by the spectrum noise. Such a behavior of the CCF is expected only if the integrated light spectrum is dominated by the contribution of the few brightest stars lying inside the area of integration (slit) of the spectrograph.

With this problem in mind we have examined the study of Peterson et al. (1989) with a great deal of attention. Two results emerge from this investigation: (1) a careful check of their results reveals a bumpy behavior of their CCF (their Fig. 10)

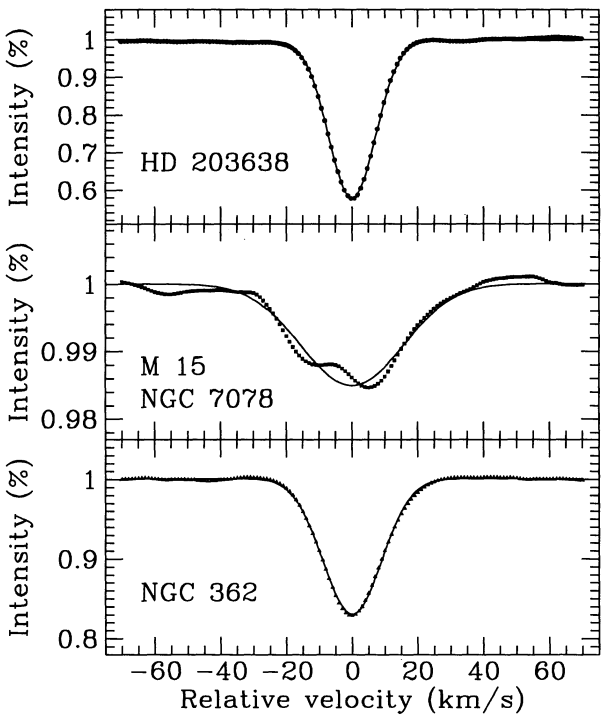

FIG. 1.—Normalized cross-correlation functions, (1) of the spectrum of HD 203638, a standard K0 giant star, (2) of the integrated light spectrum of the central 6" × 6" area in the core of M15 = NGC 7078, and (3) of the integrated light spectrum of the central 6" × 6" area in the core of another galactic globular cluster, NGC 362. The continuous lines are the corresponding fitted Gaussians. The important broadening of both cluster cross-correlation functions as well as the asymmetrical shape of the M15 cross-correlation function are conspicuous.

with departure from Gaussian shape similar to ours; (2) there are also inconsistencies in the radial velocities and velocity dispersions deduced from their different observations; as demonstrated by our numerical simulations (see § 4 below), these effects are the consequences of the fact that the integrated spectra are dominated by the light of one or two bright stars. In addition, a careful comparison of the CCF of one of their cluster spectra with a stellar CCF broadened by Gaussian functions does not allow an immediate understanding of their high velocity dispersion values (see Fig. 3 in Dubath, Mayor, & Meylan 1993).

Any integrated light spectra in the core of M15, i.e., the measurements of Peterson et al. (1989) as well as our own measurements, are strongly suspected of being dominated by the light of the few brightest stars. Peterson et al. (1989) point out this problem but make only qualitative estimates of the related errors. A quantitative estimate of the statistical errors, due to small samples, affecting the central velocity dispersion measurements of M15 is necessary for further interpretations of the results. We present in this paper detailed numerical simulations, with different integration apertures, of CCFs of integrated light spectra in the core of M15.

This paper is structured as follows: § 2 presents our observations. Section 3 describes the fact that any integrated light spectrum in the core of M15 is dominated by the contribution of the few brightest stars. Section 4 presents our numerical simulations and major results, while our conclusions are given in the last § 5.

2. OUR SPECTROSCOPIC OBSERVATIONS

A single integrated light spectrum of the core of M15 was obtained, during the night 1989 July 8–9, with CASPEC, the Cassegrain Echelle Spectrograph of the European Southern Observatory (ESO) mounted on the ESO 3.6 m telescope at La Silla, Chile. The charge coupled device (CCD) used is the ESO CCD 8. It is a RCA SID 503 high-resolution, thinned, backside illuminated device, with 1024 × 640 pixels of 15 μm square each, and with a readout noise of about 24 electrons. The instrument setup is standard, with the 31.6 line mm^{-1} grating and with a wavelength domain between 4250 and 5250 Å. The night of the observations is characterized by strong winds and seeing values of the order of 2″ FWHM. The integration time is 60 minutes, with a spectrum of a thorium-argon lamp taken before and after the exposure. The dimension of the entrance slit is 1.″2 × 6.″0. During the exposure a scanning of the nucleus was done with the entrance slit, in order to sample over a central zone of 6″ × 6″. This area of integration, represented by the large square in Figure 2, has to be compared with the cluster core diameter of 4.″4 determined from *HST* observations (Lauer et al. 1991). For our instrument setup and slit width, the typical full-width at half-maximum (FWHM) of the emission lines of the thorium-argon comparison spectra, i.e., our typical spectral resolution, is 13–14 km s^{-1}.

The spectrum is reduced following standard procedures described in detail in Dubath, Meylan, & Mayor (1994). The reduced spectrum is then cross-correlated with a numerical mask. The properties of this mask, as well as the details of our cross-correlation technique, are described in previous studies (e.g., Dubath, Meylan, & Mayor 1990, and Meylan, Dubath, & Mayor 1991a). A peculiarity of our technique resides in the fact that the template is not a spectrum but a numerical function, originally optimized for radial velocity measurements with CORAVEL (Baranne, Mayor, & Poncet 1979). The cross-correlation of a spectrum with our mask exhibits a CCF dip which is very well approximated by a Gaussian function. In the above introduction, Figure 1 displays the CCF of the spectrum of a standard K0 giant star, HD 203638, and the CCFs of the integrated light spectra in the cores of the galactic globular clusters M15 and NGC 362, respectively. The comparison of the CCF of the cluster with the CCFs of standard stars displays the broadening of the cluster CCF, produced by the Doppler line broadening present in the integrated light spectrum because of the random spatial motions of the stars.

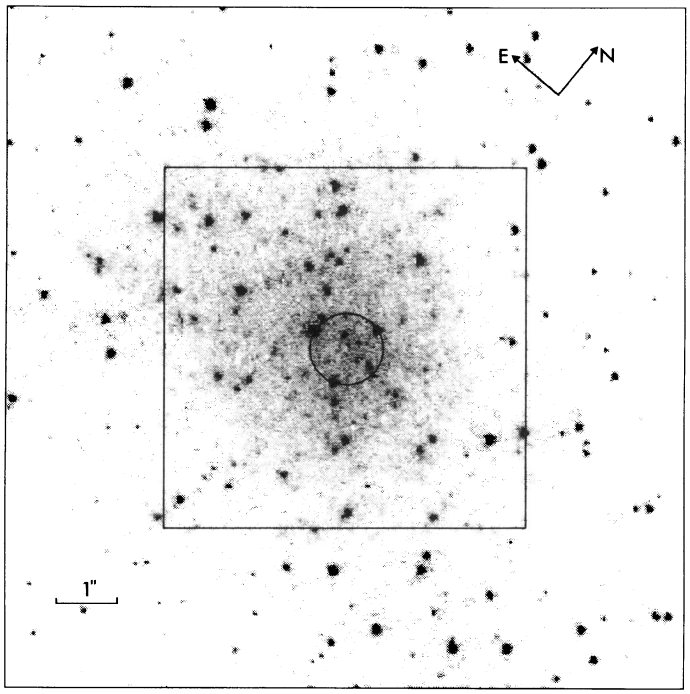

FIG. 2.—Central area containing the core of the globular cluster M15, as seen by the Faint Object Camera (FOC) of the *Hubble Space Telescope* (*HST*). This image, obtained in the F/96 mode with the F342 filter, displays an 11.″3 × 11.″3 area. The sharp cores of the point spread functions have FWHM = 0.″08. No restoration of any kind has been applied to this image. Superposed for illustration purposes are, (1) a circle of 1.″2 in diameter, representing the full aperture of the image stacker used by Peterson et al. (1989) at the MMT, and (2) a square of 6.″0 × 6.″0 corresponding to our sampling area.

The important broadening of the CCFs of both clusters is conspicuous when compared with the stellar CCF of HD 203638. The standard deviation of the intrinsic stellar cross-correlation function—$\sigma_{ref} = 7.0$ km s^{-1}—is defined by the mean value of the measurements of a sample of standard stars of appropriate spectral type. The velocity dispersion σ_p is then computed with the following equation:

$$\sigma_p^2 = \sigma_{CCF}^2(\text{cluster}) - \sigma_{ref}^2 . \quad (1)$$

Our integrated light spectrum over a central 6″ × 6″ area leads to a projected velocity dispersion $\sigma_p(0) = 14.0$ km s^{-1} (see § 4 below for a discussion of the uncertainty on this value). This determination is not significantly different from the preliminary value $\sigma_p(0) = 13.7$ km s^{-1} published by Meylan et al. (1991b).

It is worth mentioning that, because of our larger integration area, we would probably miss any central cusp in velocity dispersion. Consequently, our measurement should be equal to, or smaller than, any other measurement obtained over a smaller area. From the fact that our integration area corresponds roughly to the region inside one core radius (Lauer et al. 1991), our measurement may well be equal to any other measurement obtained over a smaller area, if the core of M15 is isothermal. Our result $\sigma_p(0) = 14.0$ km s^{-1} is in good agreement with the velocity dispersion $\sigma_p = 14.2 \pm 1.9$ km s^{-1} derived by Peterson et al. (1989) from the radial velocities of 27 stars within 20″ of the center of M15. Our result differs from their central velocity dispersion estimate; however, as the statistical errors due to small samples probably play a dominant role, an objective estimate of these errors appears necessary in order to interpret any central velocity dispersions derived from integrated light spectra.

3. SMALL NUMBER STATISTICS BECAUSE OF FEW BRIGHT STARS

Before the CFHT observations of Racine & McClure (1989) and the *HST* observations of Lauer et al. (1991), an unresolved luminosity cusp of several seconds of arc in size (marginally resolved by Aurière et al. 1984) was observed at the center of M15. Peterson et al. (1989) carried out spectroscopic observations in integrated light in order to map the kinematics of this apparent central cusp. On one hand, eight integrated light spectra were taken with the echelle spectrograph of the Multiple Mirror Telescope (MMT) at different positions on the cusp. The separation between two of these observations is of the order of 0.″8 and the effective aperture for all the observations is 1.″2. On the other hand, long-slit integrated light spectra were taken, at the 4 m telescope of Kitt Peak National Observatory (KPNO), through the central cusp and with different position angles. The slit width was 1.″0. From a cross-

correlation technique applied to the reduced spectra, corresponding to different positions in the cusp, the authors derive radial velocities from the abscissas of the peaks of the CCFs, and velocity dispersions from the broadening of the CCFs with respect to the instrumental CCF deduced from standard stars. The broadening of the CCF of an integrated light spectrum is, of course, the consequence of the Doppler shifts of photons coming from stars with different radial velocities.

The central luminosity cusp in M15 has been now resolved, partly from the ground (Racine & McClure 1989), and definitely by *HST* images (Lauer et al. 1991): it appears to be dominated by a few (essentially three) bright stars. Consequently, in the core, the integrated light spectra over effective apertures of the order of 1″ squared are expected to be dominated by the light or one or two giants. This is conspicuous from a look at Figure 2, which displays the core of M15 as seen by the Faint Object Camera (FOC) of the *HST*. This image, obtained in the F/96 mode with the F342 filter (akin to a *U* filter centered at about 3400 Å), displays an 11.″3 × 11.″3 area, with a pixel size of 0.″022. The sharp cores of the point spread functions have FWHM = 0.″08. No restoration of any kind has been applied to this image. Superposed for illustration purposes are (1) a circle of 1.″2 in diameter, representing full aperture of the image stacker used by Peterson et al. (1989) at the MMT, and (2) a square of 6.″0 × 6.″0 corresponding to our sampling area. Both the circle and the square are centered on the center of the cluster. The three bright stars just under the circle (separated from one another by about 1″) constitute the main contributors to the former luminosity cusp, not yet as clearly resolved at the time of Peterson et al.'s (1989) paper. More quantitatively, from a magnitude estimate, one sees that one or two bright stars may easily provide more than half the total light measured through an aperture of about 1.″0.

This point is clearly confirmed by two properties of the results of Peterson et al. (1989). First, the central peak of the CCF of the integrated light spectra displayed in their Figure 10 exhibits a slight but unexpected asymmetrical shape. Such a shape may naturally be explained if the integrated spectra are dominated by the light of several bright stars. This is not surprising since the same kind of bumpy shape is seen in our own data, obtained over a much larger central area but encompassing theirs. Second, their kinematical results derived from the MMT observations are inconsistent with each other: e.g., there are significant differences ($>4\ \sigma$) in radial velocities, whereas any measurements of velocity dispersion should provide always consistent radial velocity values; the velocity dispersion values exhibit also a similar inconsistency. This is illustrated in our Figure 3 where Peterson et al.'s velocity dispersions taken from their Table 4 are plotted as a function of their corresponding radial velocities; error bars are drawn from the estimates in their Table 4. The open circle in Figure 3 represents the velocity dispersion $\sigma_p = 14.2 \pm 1.9$ km s^{-1} of 27 stars within 20″ from the center as a function of the mean radial velocity $\bar{V}_r = -107.1 \pm 0.9$ km s^{-1} of the 120 stars (Peterson et al. 1989). This figure shows that the scatter of the results is very large. Again, such a large scatter in central velocity dispersion along with the inconsistencies in radial velocities may be the consequences of statistical errors due to small samples.

Peterson et al. (1989) recognize the existence and importance of these problems, but make only qualitative estimates of the related errors. They propose to disregard their lowest velocity dispersion values, attributed to the dominance of one or two bright stars. They eventually retain, as their best estimate, a lower limit of 25 ± 7 km s^{-1} for the central velocity dispersion $\sigma_p(0)$, encouraged by the fact that they obtained such a high value during each of their observing nights.

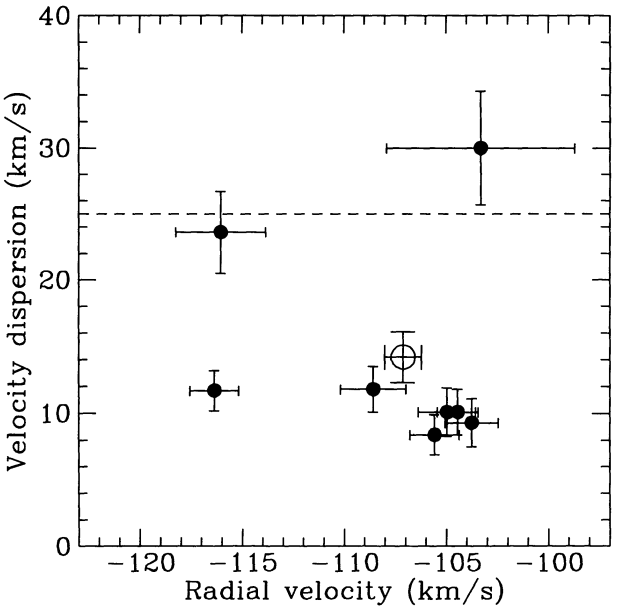

FIG. 3.—Velocity dispersion as a function of radial velocity, from the cross-correlation functions of integrated light spectra, obtained at the MMT by Peterson et al. (1989), at different positions within a few seconds of arc in the core of M15. Their velocity dispersions, taken from their Table 4, are plotted as a function of their corresponding radial velocities. Error bars are drawn following their error estimates taken from their Table 4. The large open circle is the result derived from their individual stellar measurements, i.e., the velocity dispersion $\sigma_p = 14.2 \pm 1.9$ km s^{-1} of the 27 stars within 20″ of the center as a function of the mean radial velocity $\bar{V}_r = -107.1 \pm 0.9$ km s^{-1} of the 120 stars. The dashed horizontal line represents the central velocity dispersion adopted by Peterson et al. (1989).

4. NUMERICAL SIMULATIONS

Extensive numerical simulations are carried out in order to estimate the influence of statistical error due to a small sample on radial velocity and velocity dispersion determinations, when derived from the CCFs of integrated light spectra. By definition, an integrated light spectrum is the sum of all the spectra of the stars which appear inside the area of integration, in projection on the plane of the sky. Such a spectrum may be reproduced, numerically, by adding stellar spectra of appropriate MK spectral types, each of them shifted in wavelength by a small amount in order to simulate the spatial random motions of the stars. Simulations of such spectra have been carried out by Zaggia et al. (1992a, b, 1993).

The above type of simulations is CPU time consuming. Alternatively, the CCFs of integrated light spectra may be directly simulated by adding stellar CCFs adequately shifted in velocity. The CCF of a template with a sum of spectra is equal to the sum of the CCFs of the template with each spectrum. As our cross-correlation technique produces a CCF which is nearly a perfect Gaussian, we simply add Gaussian functions to reproduce CCFs of integrated light spectra. The present way of simulating the CCF of integrated light spectra is much less CPU time consuming than when actually achieving the cross-correlation of a sum of stellar spectra; it makes it possible to carry out a very large number of simulated CCFs ($>100{,}000$) in a reasonable amount of time.

Since our numerical simulations will be used in some forthcoming studies of other galactic and Magellanic clusters, a rather detailed description of the ingredients of our simulations is given below. The reader interested only in the results of these simulations may skip §§ 4.1, 4.2, and 4.3, and read directly §§ 4.4 and 4.5.

4.1. *Ingredients of the Simulations*

Let us first call to mind some properties of our cross-correlation technique. With our method, the CCF can be considered as the average profile of all the weak spectral lines present in the spectrum of the star (see § 3.3 of Dubath et al. 1990). Mayor (1980) shows that, with CORAVEL measurements of a sample of F and G dwarf stars, the total area W_{CCF} of the cross-correlation function dip is essentially a function of both the metal abundance and effective temperature of the star observed. A similar relation exists also for the giant stars. Given the strong similarities between CORAVEL and our numerical technique, we expect the above relations to be valid also in the present case. Of course we have carefully checked, with numerous standard star measurements over several observing runs, that the CCFs from both approaches (CORAVEL and numerical) do indeed have similar behaviors.

In the case of a globular cluster, whose stars have approximately the same metallicity, the total area of the CCF depends only on the effective temperature of the star. From the work of Mayor (1980), we derive a relation which allows to estimate W_{CCF} as a function of the color index $B-V$ of the star. Because the CCF is a Gaussian function, the total area W_{CCF} of the CCF is related to its depth D_{CCF} and to its standard deviation σ_{CCF} by the following relation: $W_{CCF} = D_{CCF}\,\sigma_{CCF}\,(2\pi)^{1/2}$.

The standard deviation σ_{CCF}, or width, of the CCF is related to the average of the widths of the spectral lines considered. These widths depend on the intrinsic line widths and on the resolution of the spectroscopic observations. Because the line broadening mechanisms (e.g., rotation and macroturbulence) are not effective in the bright stars of globular clusters, the intrinsic widths of their spectral lines are relatively small. As a consequence, the observed line widths and the FWHM of the CCFs of such stars, depend mainly on the spectral resolution of the observations, and can be considered as constant for all these stars. A standard deviation—$\sigma_{ref} = 7.0$ km s^{-1}—of the CCF, defined as the mean of the standard deviations of all our observed CCFs of a sample of five K giant stars, is used for all the simulations. The depth D_{CCF} of the CCF becomes a function of the color of the star only, and can be written

$$D_{CCF} = \frac{W_{CCF}}{\sigma_{ref}\sqrt{2\pi}}\,. \qquad (2)$$

In order to achieve our simulations, we need, ideally, both the luminosity function and the color-magnitude diagram of M15. The published parts of the luminosity function of M15 cover, unfortunately, either the luminosity range from the bright end to the faint part of the giant branch (e.g., Buonanno, Corsi, & Fusi Pecci 1985; Sandage, Katem, & Kristian 1968) or the luminosity range from the top of the main sequence down to the faintest measured stars (e.g., Fahlman & Richer 1985; Sandage & Katem 1977). There is an observational gap between these two luminosity ranges, around the magnitudes concerning turnoff and subgiant stars. The luminosity function of M92 is arbitrarily used to circumvent this problem. This cluster is chosen because (1) its metallicity is similar to the metallicity of M15, (2) the luminosity functions found in the literature for both clusters agree reasonably well over the common ranges, and (3) its luminosity function from Hartwick (1970) covers a large enough luminosity range (from 11.9 to 21.1 in V magnitude) to encompass all M15 luminosity ranges. This M92 luminosity function is transformed into a luminosity function in absolute magnitude M_V by using an uncorrected distance modulus $(m-M)_V = 14.6$ taken from Stetson & Harris (1988).

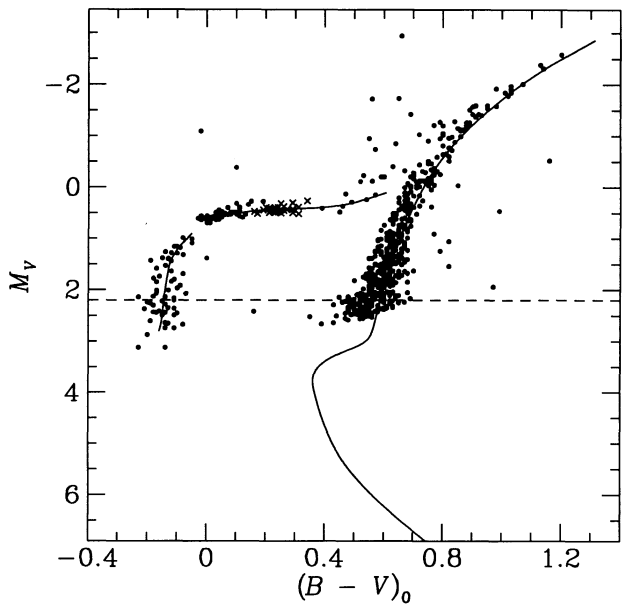

FIG. 4.—Color-magnitude diagram of M15, M_V vs. $(B-V)_0$, used in our simulations. The dots represent the stars from Buonanno et al. (1985), and the crosses represent the mean M_V and $(B-V)_0$ of the RR Lyrae stars from Bingham et al. (1984). This diagram is complete down to an absolute magnitude $M_V = 2.2$, a limit illustrated by the horizontal dashed line. The solid lines drawn on this figure are the M15 fiducial sequences taken from Fig. 21 of Hesser et al. (1987).

Figure 4 presents the M15 color-magnitude diagram, M_V versus $(B-V)_0$, used for our simulations. The dots represent the positions of the stars from Buonanno et al. (1985), and the crosses represent the mean M_V and $(B-V)_0$ of the RR Lyrae stars taken from Bingham et al. (1984). The transformation of V and $B-V$ into M_V and $(B-V)_0$ is made by using an uncorrected M15 distance modulus $(m-M)_V = 15.4$ and a reddening $E(B-V) = 0.11$ (Hesser et al. 1987). This diagram is complete down to an absolute magnitude $M_V = 2.2$, a limit illustrated in Figure 4 by the horizontal dashed line. The solid curves drawn on this figure are the M15 fiducial sequences taken from Figure 21 of Hesser et al. (1987).

4.2. *Simulation of the CCF of One Particular M15 Star*

The cross-correlation function of a star of M15 is simulated by performing the following four steps:

1. First, the absolute magnitude M_V is randomly assigned to the simulated star, using the M92 luminosity function covering the range 11.9 to 21.1 in V, i.e., −2.7 to 6.5 in M_V. Then:

If M_V is brighter than 2.2, an absolute V-magnitude is reassigned to the star, together with a color index $(B-V)_0$, by selecting randomly one star with $M_V < 2.2$ in the M15 color-magnitude diagram (Fig. 4).

If M_V is fainter than 2.2, the original magnitude is conserved, and a color index $(B-V)_0$ is assigned to the star by

using the fiducial main sequence of the M15 color-magnitude diagram (Fig. 4). The few stars on the horizontal branch lying below $M_V = 2.2$ are ignored in the present simulation.

2. The depth D_{CCF} of the CCF is then attributed to the star by using its color index. If $(B-V)_0 > 0.3$, D_{CCF} is given by equation (2); if $(B-V)_0 < 0.3$, equation (2) is no longer valid and D_{CCF} is set to zero, since we know from previous experience that such stars [bluer than $(B-V)_0 = 0.3$] have CCFs of negligible depths.

3. In order to take into account the spatial motion of the stars inside the cluster, a radial velocity V_r^{star} is randomly assigned to each star, by using a Gaussian velocity distribution of mean value equal to zero and of standard deviation equal to the input velocity dispersion σ_{in} of the corresponding simulated CCF, i.e., the value, of a given simulated CCF, representing the true velocity dispersion of the cluster.

4. As the CCF is assumed to be a Gaussian, itself a function of the velocity v, it can now be computed from the following equation:

$$CCF(v) = 10^{M_V/2.5}\left\{1 - D_{CCF} \exp\left[-\frac{(V_r^{star} - v)^2}{2\sigma_{ref}^2}\right]\right\}, \quad (3)$$

where the different parameters M_V, D_{CCF}, V_r^{star}, and σ_{ref} have the values assigned above.

4.3. *Simulation of the CCFs of Integrated Light Spectra of M15*

In order to simulate the CCF of an integrated light spectrum of M15, a large number N_s of CCFs of simulated M15 stars given by equation (3) are summed together. In a way identical to the case of a genuine observed CCF, a Gaussian function is fitted to this simulated CCF in order to determine: (1) the abscissa of its minimum, i.e., its radial velocity V_r, (2) its depth D_{CCF}, and (3) its standard deviation σ_{CCF}. The velocity dispersion σ_{out} resulting from the simulated CCF is given from equation (1) by $\sigma_{out}^2 = \sigma_{CCF}^2 - \sigma_{ref}^2$. In order to take into account the statistical variations of the number of stars appearing inside the area of integration, the total number N_s of summed stars is not taken constant from one simulated CCF to another. For a particular simulated CCF, N_s is randomly determined from a Gaussian distribution of mean value equal to N and of standard deviation $\sigma = N^{1/2}$. Therefore, in a set of simulated CCFs, the number of summed stars N_s varies from one simulated CCF to another, and N represents the mean of the different N_s values. The sum of the apparent V magnitudes of the N_s stars considered gives the total magnitude m_V^{tot} corresponding to a particular simulated CCF. The mean total magnitude obtained from a set of simulated CCFs has to be compared with the observed magnitude of the total light coming from the area of integration: they should match each other.

Peterson et al. (1989) estimate, within their 1.″2 aperture, a total quantity of light equal to 13.0 V-magnitudes. In order to derive the magnitude through our larger aperture of 6″ × 6″, the integrated V radial surface-brightness profile of Newell & O'Neil (1978) is used. A V-magnitude of 10.7 is obtained for a central area of 36″ squared. The V profiles of Newell & O'Neil (1978) and Aurière & Cordoni (1981), and the U profiles of Newell & O'Neil (1978) and Lauer et al. (1991) are displayed in Figure 5. All profiles appear to be in relatively good agreement, and display the same structural shape. This gives some confidence in the reliability of our V-magnitude estimates, although they probably suffer from statistical noise because of too small a number of bright stars present in the cluster center. center.

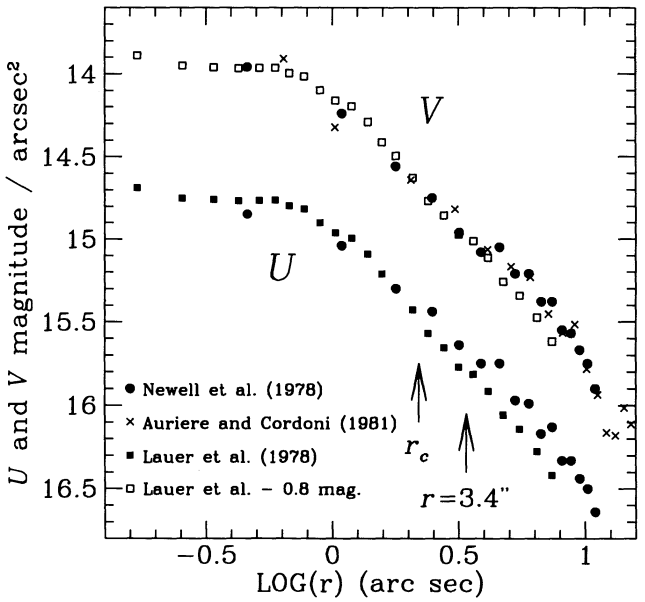

FIG. 5.—Comparison of the published U and V profiles in the central part of M15: the V profiles are from Newell & O'Neil (1978) and Aurière & Cordoni (1981), and the U profiles from Newell & O'Neil (1978) and Lauer et al. (1991). The vertical arrow marked with r_c represents the core radius of 2.″2 = 0.13 pc determined by Lauer et al. (1991). The vertical arrow marked with 3.″4 represents the radius of a disk with a surface equal to the surface of our squared sampling area of 6″ × 6″.

A large number (>100,000) of simulated CCFs, with N (the mean number of summed stars for one CCF) equal to 300 and 2200 stars, lead to total magnitudes m_V^{tot} whose distributions have means and standard deviations equal to 13.0 ± 0.4 and 10.8 ± 0.2, respectively. Both mean total magnitudes match well the magnitudes obtained inside the two considered apertures of size equal to 1″ × 1″ and 6″ × 6″, respectively. Therefore, in the following discussion, the numbers of stars $N = 300$ and $N = 2200$ are associated with the magnitudes 13.0 and 10.8, corresponding to the small and large apertures, respectively.

The input parameters for a set of simulated CCFs are the mean number N of summed stars and the input velocity dispersion σ_{in}. For each couple of values $[N; \sigma_{in}]$, a large number of simulated CCFs, typically 5000 to 10,000 CCFs, are achieved. Each set of simulated CCFs produces, (1) a distribution of the total numbers of summed stars N_s, (2) a distribution of the total magnitudes m_V^{tot} of the N_s stars, (3) a distribution of the ratios of giant to dwarf stars with $M_V = 2.2$ as limiting absolute magnitude, (4) a distribution of the velocities V_r, (5) a distribution of the CCF depths D_{CCF}, and (5) a distribution of the velocity dispersions σ_{out}. The above distributions (2) and (3) are given by the generation of M_V from the luminosity function and the color magnitude diagram, whereas the above distributions (4), (5), and (6) come from the fits of Gaussians to the simulated CCFs.

4.4. *Results of the Simulations: Qualitative Behavior*

In Figure 6, a set of 24 simulated CCFs obtained with $N = 2200$ stars (integration area of 6″ × 6″) and $\sigma_{in} = 15$ km s^{-1} are displayed together with our genuine observed CCF of

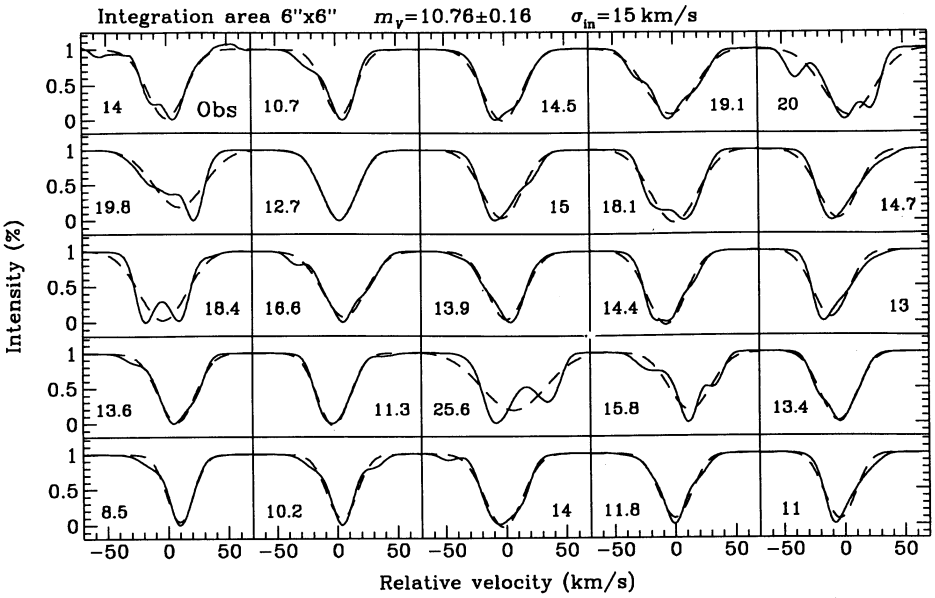

FIG. 6.—Set of 24 simulated CCFs obtained with $N = 2200$ stars (integration area of 6″ × 6″) and $\sigma_{in} = 15$ km s^{-1}, together with our observed CCF of M15 (*upper left panel*). The continuous lines are the CCFs themselves, and the dashed lines are the fitted Gaussians. In each panel, the velocity dispersion σ_{out} obtained from the Gaussian fit to the CCF is indicated in km s^{-1}.

M15 (*upper left panel*). The continuous lines are the CCFs themselves, and the dashed lines are the fitted Gaussians. In each panel, the velocity dispersion σ_{out} obtained from the Gaussian fit to the CCF is indicated in km s^{-1}. These CCFs have not been selected in any way, but represent a random succession of 24 of the simulated CCFs. This sample of CCFs shows that the noisy shape of our observed CCF of M15 (Fig. 1) is qualitatively easily reproduced by the simulations.

Figure 7 displays, on two rows, the velocity dispersion distributions resulting from eight different sets of simulated CCFs. The first row displays the four distributions of the velocity dispersions σ_{out}, as clear histograms, for four sets of 10,000 simulated CCFs, characterized by the following input parameters: 300 stars (integration area of 1″ × 1″) and $\sigma_{in} = 10$, 15, 20, and 25 km s^{-1}, from left to right, respectively. These input parameters are indicated in each diagram. The observed velocity dispersion values from Peterson et al. (1989), corresponding to this 1″ × 1″ integration area, are represented as the crosshatched histograms; the ordinate scales of the two histograms (clear and crosshatched) are very different, since only seven measurements (the two measurements in position C having been averaged) are represented in the crosshatched ones. The upward arrow represents the input velocity dispersion σ_{in} of the simulation, and the downward one represents the average $\bar{\sigma}_{out}$ of the distribution (clear histogram) of the velocity dispersions σ_{out} resulting from the simulations. The second row displays the distributions of the velocity dispersions σ_{out}, as clear histograms, for four sets of 6000 simulated CCFs, characterized by the following input parameters: 2200 stars (integration are of 6″ × 6″) and $\sigma_{in} = 10$, 15, 20, and 25 km s^{-1}, from left to right, respectively. These input parameters are indicated in each diagram. Our observed velocity dispersion—$\sigma_p(0) = 14.0$ km s^{-1}—from § 2 above, corresponding to this 6″ × 6″ integration area, is represented as the crosshatched histograms, made of one measurement only. The upward and downward arrows represent again σ_{in} and $\bar{\sigma}_{out}$ values, respectively. The dashed curves are Gaussian functions fitted to the clear histograms.

Figure 7 conspicuously shows that statistical variations of the output velocity dispersion σ_{out} resulting from the simulations are very important. For example, from the first row, we see that if the input central velocity dispersion $\sigma_{in} = 20$ km s^{-1}, the simulations of measurements over an area of 1″ squared produce velocity dispersions which range from about 2 to 25 km s^{-1}, because too few stars dominate the integrated light. From the second row, i.e., in cases concerning a much larger integration area of 36″ squared, this range is not much smaller. Quantitatively, this range does not decrease with $N^{1/2}$ as one could have naively thought. The simulations with $N = 300$ stars (integration are of 1″ × 1″) lead to wide and strongly asymmetric distributions of velocity dispersions, with a $\bar{\sigma}_{out}$ which is lower than the input velocity dispersion σ_{in}. When N increases, the distributions become narrower and more symmetric. With $N = 2200$ stars (integration are of 6″ × 6″) the distributions become nearly Gaussian and their mean values $\bar{\sigma}_{out}$ are much closer to σ_{in}. From the upper to lower row of Figure 7, i.e., with an increasing number of stars (from 300 to 2200 stars), the widths of the distributions decrease only slowly. From the left to the right column of the same figure, i.e., with an increasing σ_{in}, (from 10, 15, 20, to 25 km s^{-1}) the distributions widen strongly.

The two general behaviors—(1) the distributions become slowly narrower and nearly Gaussian as the number of stars N (i.e., the aperture) increases, and (2) distributions widen strongly as σ_{in} increases—may be understood from the following few considerations.

The luminosity function of a globular cluster decreases sharply with luminosity. The contribution of a given group of stars (e.g., defined by an interval in V-magnitude) to the total light of the cluster may be estimated from the luminosity function and the typical stellar luminosity of the group. As a result, the contribution in luminosity of the few brightest stars is of

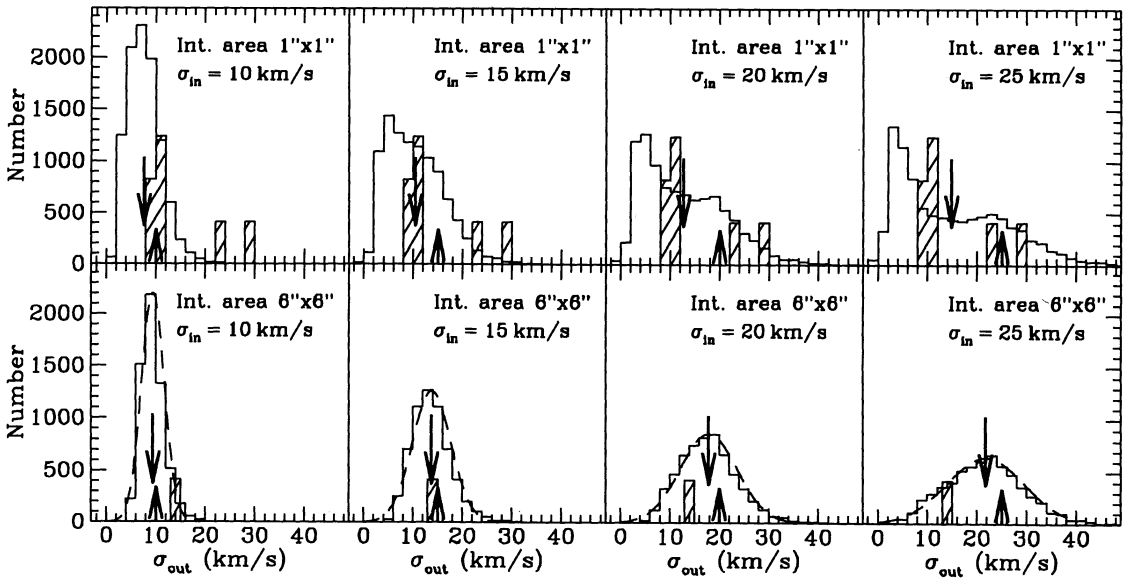

FIG. 7.—Distributions of velocity dispersions σ_{out} resulting from eight different sets of simulated CCFs. The first row displays the distributions of the velocity dispersion σ_{out} as clear histograms, for four sets of 10,000 simulated CCFs, characterized by the following input parameters: 300 stars (integration area of 1″ × 1″) and σ_{in} = 10, 15, 20, and 25 km s^{-1}. These input parameters are indicated in each diagram. The observed velocity dispersions from Peterson et al. (1989), corresponding to this 1″ × 1″ integration area, are represented as the crosshatched histograms; the ordinate scale of the two histograms (clear and crosshatched) are very different, since only seven measurements are represented in the crosshatched ones. The upward arrow represents the input velocity dispersion σ_{in} of the simulation, and the downward one represents the average $\bar{\sigma}_{out}$ of the distribution (*clear histogram*) of the velocity dispersions σ_{out} resulting from the simulations. The second row displays the velocity dispersion distributions, as clear histograms, for four sets of 6000 simulated CCFs, characterized by the following input parameters: 2200 stars (integration area of 6″ × 6″) and σ_{in} = 10, 15, 20, and 25 km s^{-1}. These input parameters are indicated in each diagram. Our observed velocity dispersion, corresponding to this 6″ × 6″ integration area, is represented as the crosshatched histograms, made of one measurement only. The upward and downward arrows represent again σ_{in} and $\bar{\sigma}_{out}$ values, respectively. The dashed curves are Gaussian functions fitted to the clear histograms.

the same order of magnitude as the contribution of the much more numerous fainter stars. Therefore, the few brightest stars lying in the area of integration, have a strong influence on the shape of the cross-correlation function. If the brightest star in the spectrograph slit is much brighter than the second brightest star, its contribution is dominant and the velocity dispersion may be underestimated, the CCF having a stellar profile (see leftmost panel of the lowest row in Fig. 6). Alternatively, the velocity dispersion may also be overestimated if the two brightest stars have similar luminosities and are well separated in terms of radial velocity, widening the cross-correlation function (see middle panel of the fourth row in Fig. 6). Both cases happen in the simulations. However, the second case is less frequent than the first one, making the distribution of resulting velocity dispersions asymmetrical, i.e., skewed toward small values, as visible from the upper row of Figure 7. When the number of stars N (i.e., the aperture) increases the situation does not improve dramatically, because the statistics of the few brightest stars remain nearly unchanged. These stars are on average brighter, but they still come from a sharply decreasing part of the luminosity function. The luminosity ratio of the brightest star to the second or third brightest star does not depend strongly on the number N of stars considered. Nevertheless, the distributions of output velocity dispersions narrow slowly with N and become more and more symmetric, as visible from the lower row of Figure 7. This last point indicates that the case where one star is clearly dominant is much less frequent with large values of N.

Figure 8 is an illustration of the behavior of the simulated cross-correlation functions obtained with a small number of stars, in the different cases of under- and overestimates of the velocity dispersion. It displays 25 different simulated CCFs, with N = 300 stars (integration area of 1″ × 1″) and σ_{in} = 25 km s^{-1}. In these simulations, our usual intrinsic stellar cross-correlation function σ_{ref} = 7.0 km s^{-1} has been replaced by σ_{ref} of 8.7 km s^{-1} in order to match the slightly lower spectral resolution of the observations of Peterson et al. (1989). As in Figure 6, the continuous lines are the cross-correlation functions themselves, and the dashed lines are the fitted Gaussians. In each panel, the velocity dispersion σ_{out} obtained from the Gaussian fit to the cross-correlation function is indicated in km s^{-1}. The cross-correlation functions, obtained from a random succession of 25 simulated CCFs, have been sorted (by column) as a function of σ_{out}, from the narrowest to the widest. Schematically, the cross-correlation functions belong to two different classes: (1) the narrow ones, occupying the left three columns, for which the cross-correlation function is clearly dominated by the brightest star, and (2) the wide ones, most of them exhibiting a bimodal behavior. Both effects are less pronounced in the examples of Figure 6, because of the larger number of summed stars N and the smaller value of σ_{in}, however the widest cross-correlation functions are also the noisiest, in agreement with the above argument.

When the input velocity dispersion σ_{in} is large, the cross-correlation functions of the few brightest stars are stretched over a larger velocity range, making the total cross-correlation function noisier and increasing the influence of the luminosity variation of the few brightest stars. A particular case, which becomes more and more frequent with increasing σ_{in}, is when the cross-correlation function dips of particular bright stars, have large relative velocities with respect to the main cross-correlation function dip of the bulk of the summed stars. Such secondary dips have small weights in the fitting process, as clearly shown by the two examples labeled A and B in Figure

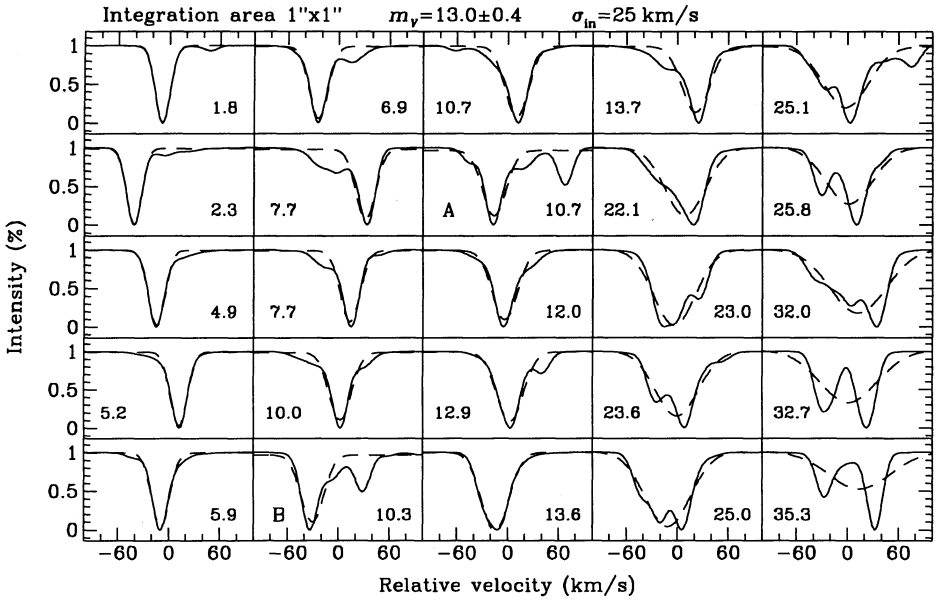

FIG. 8.—Set of 25 simulated CCFs obtained with $N = 300$ stars (integration area of 1″ × 1″) and $\sigma_{in} = 25$ km s^{-1}. As in Fig. 6, the continuous lines are the CCFs themselves, and the dashed lines are the fitted Gaussians. In each panel, the velocity dispersion σ_{out} obtained from the Gaussian fit to the CCF is indicated in km s^{-1}. The CCFs, obtained from a random succession of 25 simulated CCFs, have been sorted (by column) as a function of σ_{out}, from the narrowest to the widest.

8: as a consequence, the velocity dispersion is severely underestimated.

4.5. *Results of the Simulations: Error Estimates*

The input velocity dispersion σ_{in} represents, in the simulations, the cluster true (projected) velocity dispersion σ_p, i.e., the quantity we try to measure. The output velocity dispersion σ_{out} represents in the simulations the measured velocity dispersion. The distribution of the output velocity dispersions σ_{out} (Fig. 7) can be considered as a probablity distribution, giving the probability of obtaining a particular value σ_{out} from an integrated light measurement over the considered sampling area if the input velocity dispersion is σ_{in}. In order to estimate the errors on the velocity dispersions derived from observations in integrated light spectra, the observed velocity dispersions have to be compared with the distribution of velocity dispersions σ_{out} resulting from the simulations (Fig. 7).

The results of the simulations already shown in Figure 7 are presented in a different way in Figure 9, where $\bar{\sigma}_{out}$ is given as a function of σ_{in} (both quantities correspond in Fig. 7 to the downward and upward arrows, respectively). In the left diagram of Figure 9, the four dots represent, in the case $N = 300$ stars (integration area of 1″ × 1″), the averages $\bar{\sigma}_{out}$ of the velocity dispersions σ_{out} obtained in the four cases from 10,000 simulated CCFs, as a function of the input velocity dispersion $\sigma_{in} = 10$, 15, 20, and 25 km s^{-1}. The error bars

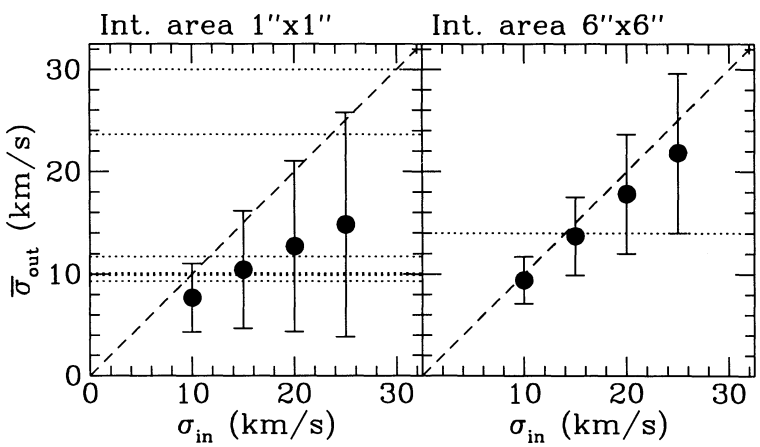

FIG. 9.—$\bar{\sigma}_{out}$ vs. σ_{in}: in the left diagram, in the case $N = 300$ stars (integration area of 1″ × 1″), the dots represent the averages $\bar{\sigma}_{out}$ of the velocity dispersions σ_{out}, ovet the 10,000 simulated CCFs, as a function of the input velocity dispersion $\sigma_{in} = 10$, 15, 20, and 25 km s^{-1}. The error bars represent the standard deviations of the derived velocity dispersion σ_{out}. As $\bar{\sigma}_{out}$ is always smaller than σ_{in}, one sees that on average, integrated light measurements over such a small area lead to an underestimation of σ_p. The dashed horizontal lines represent the original velocity dispersions of Peterson et al. (1989). The right diagram represents also $\bar{\sigma}_{out}$ as a function of σ_{in}, but in the case $N = 2200$ stars (integration area of 6″ × 6″), as a function of the input velocity dispersion $\sigma_{in} = 10$, 15, 20, and 25 km s^{-1}. The dashed horizontal line represents our determination of the velocity dispersion. The fact that the underestimate of σ_p becomes significantly smaller is a direct consequence of the use of a larger integration area.

represent the standard deviations of the means of the velocity dispersions σ_{out} derived from the velocity distributions (Fig. 7). As $\bar{\sigma}_{out}$ is always smaller than σ_{in}, one sees that, *on average*, the integrated light measurements over small areas of the order of a few seconds of arc squared lead to an underestimation of the true cluster velocity dispersion σ_p. The dashed horizontal lines represent the velocity dispersions of Peterson et al. (1989), i.e., correspond to the values of the crosshatched histograms of Figure 7. The right diagram represents also $\bar{\sigma}_{out}$ as a function of σ_{in}, but in the case $N = 2200$ stars (integration area of $6'' \times 6''$), as a function of the input velocity dispersion $\sigma_{in} = 10$, 15, 20, and 25 km s^{-1}. In this diagram, the single dashed horizontal line represents our determination of the velocity dispersion. The underestimate of σ_p, significantly smaller, is a direct consequence of the use of a larger integration area.

The two diagrams of Figure 9 illustrate the statistical errors due to small samples, associated with the different measurements of σ_p and given by the range of input velocity dispersion σ_{in}, for which the simulations produce, with a reasonable probability, output apparent velocity dispersions σ_{out} compatible with the observations. However, for quantitative estimates of these errors we need to know, as a function of σ_{in}, the number of times that the simulations produce an output velocity dispersion σ_{out} about equal to the observed value σ_p, i.e., the frequency distribution along an horizontal line in this Figure 9. In order to derive these frequency distributions, one counts the number of times that a set of simulated CCFs produces a σ_{out} about equal to the observed velocity dispersion. This calculation is repeated for different sets of simulated CCFs—all sets with the same number of simulated CCFs—characterized by the two following parameters: (1) a number of summed stars corresponding to the aperture of the considered observation, identical for all sets, and (2) a different input velocity dispersion σ_{in} for each set. The number of times that a set produces a given σ_{out}, as a function of σ_{in}, gives the probability distribution of the true velocity dispersion of the cluster σ_p—represented by σ_{in}—associated with an oberved velocity dispersion equal to σ_{out}.

We have carried out 35 sets of 5000 simulated CCFs, with N equal to 300 stars (integration area of $1'' \times 1''$) and σ_{in} ranging from 6 to 40 km s^{-1} by intervals of 1 km s^{-1}, and 31 sets of 5000 simulated CCFs, with N equal to 2200 stars (integration area of $6'' \times 6''$) and σ_{in} ranging from 6 to 36 km s^{-1} by intervals of 1 km s^{-1}. The first row of Figure 10 displays, for the sets of simulations with $N = 300$ stars, the number of simulated CCFs which produce $\sigma_{out} = 10 \pm 0.75$, 15 ± 0.75, 20 ± 0.75, 25 ± 0.75 km s^{-1}, from left to right, respectively, as a function of σ_{in}. The second row displays similar histograms but for the sets of simulated CCFs with $N = 2200$. The parameters of each simulation are indicated in each diagram. In order to check that the shape of these histograms does not depend much on the width of the window taken around the σ_{out} considered (i.e., ± 0.75 km s^{-1}), the histograms obtained through a narrower window equal to ± 0.25 km s^{-1} are scaled up by a factor of 3 for comparison and displayed as dotted histograms in each diagram. The shapes are identical in all cases.

The shape of the above distributions exhibits a slow dependence on the numbers N of summed stars (i.e., on the size of the integration area), whereas it is very sensitive to the output velocity dispersion σ_{out} considered.

In order to compute the statistical error due to a small sample on the observed velocity dispersion in the core of M15, we first consider our result of $\sigma_p = 14$ km s^{-1} obtained with an area of integration of $6'' \times 6''$. Ideally, the error estimate should be given by the standard deviation of the probability distribution displayed in Figure 10. In the present case, from a pure mathematical point of view, none of the simulated probability distributions is integrable because none of them tends to zero as σ_{in} increases, preventing any estimate of the standard deviation. Instead of the standard deviation, we use the half-width at half-maximum (HWHM). From the maximum and HWHM of the probability distributions of σ_{in} obtained with σ_{out} equal

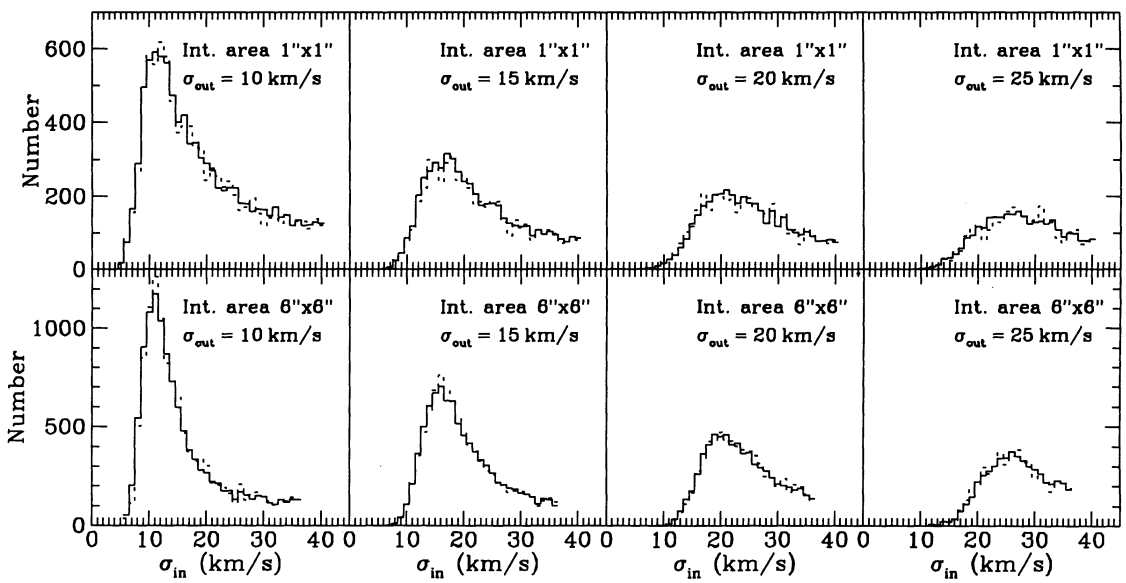

FIG. 10.—Frequency distributions of the number of times that a set of 5000 simulated CCFs produces a given σ_{out}, as a function of σ_{in}. The first row displays, for the sets of simulations with $N = 300$ stars, the number of simulated CCFs which produce $\sigma_{out} = 10 \pm 0.75$, 15 ± 0.75, 20 ± 0.75, 25 ± 0.75 km s^{-1}, from left to right, respectively, as a function of σ_{in}. The second row displays similar histograms but for the sets of simulated CCFs with $N = 2200$. The parameters of each simulation are indicated in each diagram.

to the above σ_p (this distribution is akin to those in the diagrams of Fig. 10) we derive $\sigma_p = 15^{+6}_{-4}$ km s^{-1} over an area of integration of 6″ × 6″.

A quantitative estimate of the statistical errors due to small samples in the results of Peterson et al. (1989) cannot be directly deduced from our simulations, our cross-correlation techniques being not exactly similar. Nevertheless, simulations adapted to their case ($N = 300$ stars, integration area of 1″ × 1″), suggest that the sampling errors in their results are larger than in our case. Figure 7 shows that any central velocity dispersion between 15 km s^{-1} and any arbitrary larger value can explain, as an input value to the simulations, the distribution of the seven independent velocity dispersion measurements made around the cluster center by Peterson et al. (1989). A similar result is obtained by Zaggia et al. (1993) on the basis of numerical simulations achieved with a more standard cross-correlation technique.

The statistical errors due to small samples are so large that they clearly dominate all other kinds of measurement errors, e.g., due to photon counting noise and CCD readout noise, which can be estimated to be of the order of 1–2 km s^{-1}. The latter can therefore be ignored in the present discussion. The errors on the general astrophysical parameters have no significant influence on the present simulations: from different determinations found in the literature, the uncertainties on the input parameters $(m-M)_V$ of M92, $(m-M)_V$, and $E(B-V)$ of M15 may be estimated to be about 0.1–0.2 mag and do not affect significantly the results of our simulations. These simulations and the deduced results appear almost insensitive to small changes (as large as 50%) of the total number N of summed stars, therefore, the conclusions of this work do not suffer from the existing uncertainties on the magnitude estimates of the total light coming through the different apertures.

5. SUMMARY AND CONCLUSION

A projected velocity dispersion $\sigma_p(0) = 14.0$ km s^{-1} is derived from an integrated light spectrum obtained at the European Southern Observatory (ESO) at La Silla, Chile, over a central 6″ × 6″ area in the core of the globular cluster M15. Extensive numerical simulations, prompted by the bumpy behavior of the cross-correlation function, show that all the velocity dispersions obtained from integrated light measurements over small central areas suffer from large statistical errors due to the small numbers of bright stars present in the integration area. These simulations, over our area of integration of 6″ × 6″, give $\sigma_p = 15^{+6}_{-4}$ km s^{-1} as the most probable values for the central velocity dispersion and its statistical error.

Our result contrasts with the Peterson et al. (1989) claim that the central velocity dispersion in M15 is larger than 25 km s^{-1}. However, their eight independent velocity dispersion measurements, which were obtained over integration areas of about 1″ × 1″ around the cluster center with values ranging from 8.4 to 30 km s^{-1}, have a distribution which can simply result from the fact that one or two giants dominate the light in such a small integration area. Qualitatively, their six velocity dispersion measurements comprised between 8.4 and 11.8 km s^{-1} underestimate the velocity dispersion because the light from one star dominates the integrated light: the cross-correlation functions are too narrow since they are of stellar widths. The two highest values of the velocity dispersion, viz. 23.6 ± 3.1 and 30.0 ± 4.3 km s^{-1}, may result from spectra in which the integrated light is dominated by the contributions from two stars of similar brightnesses but very different radial velocities: the cross-correlation functions are artificially broadened.

A quantitative estimate of the statistical errors due to small samples in the results of Peterson et al. (1989) cannot be directly deduced from our simulations, our cross-correlation techniques being not exactly similar. Nevertheless, simulations adapted to their case (integration area of 1″ × 1″), suggest that the statistical errors in their results are larger than in our case. This is in agreement with similar statistical error estimates carried out by Zaggia et al. (1993). Given these large uncertainties, all velocity dispersion estimates are not significantly different from $\sigma_p(0) \sim 15$ km s^{-1}. The significance of the observational evidence for a central cusp in velocity dispersion in the core of the globular cluster M15 is very low. Further work is clearly needed in order to confirm, or disprove, if the central velocity dispersion in M15 is significantly larger than the about 16 km s^{-1} expected if the core of M15 is isothermal.

Figure 11 displays twice the velocity-dispersion profile of M15, as a function, first, of the radius and, second, of the logarithm of the radius, in minutes of arc. The filled circles represent the values derived from measurements of individual

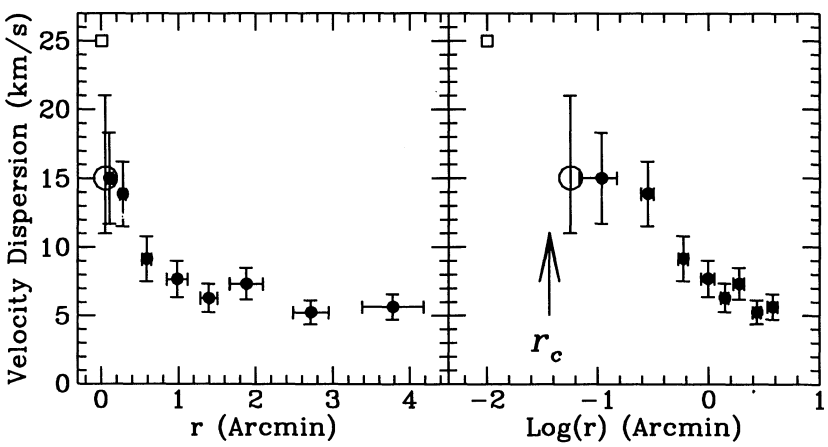

FIG. 11.—Velocity-dispersion profile of M15, as a function, first, of the radius and, second, of the logarithm of the radius, in minutes of arc. The filled circles represent the values derived from measurements of individual stars by Peterson et al. (1989), the open square represents their adopted central velocity dispersion, and the open circle represents our own measurement.

stars by Peterson et al. (1989), the open square represents their adopted value for the central velocity dispersion (25 km s^{-1}), and the open circle our own measurement (14.0 km s^{-1}). Taking into account the large uncertainties of the central velocity dispersion estimates, the velocity-dispersion profile of M15 may well flatten down at a value of about 15–16 km s^{-1} within the central $\sim 5''$, i.e., over an area which in radius is twice as large as the cluster core radius—$r_c = 2''.2$—derived from the *HST* observations (Lauer et al. 1991). This velocity-dispersion profile is consistent with various theoretical dynamical models of M15, in particular with the predictions of central velocity dispersions of: $\sigma_p(0) = 12$–17 km s^{-1} from Illingworth & King (1977), $\sigma_p(0) = 13$–15 km s^{-1} from Phinney & Sigurdsson (1991) and Phinney (1993), and $\sigma_p(0) = 14$ km s^{-1} from Grabhorn et al. (1992). Consequently, there is no need to invoke the presence of any massive central black hole.

It is a pleasure to thank the staff of the European Southern Observatory at La Silla (Chile) for their help during our observing runs. Many thanks to D. Macchetto and F. Paresce for permitting us to use the image of the core of M15 taken by the European Space Agency's Faint Object Camera on the *Hubble Space Telescope*. The Swiss National Science Foundation is acknowledged for partial financial support.

REFERENCES

Aurière, M., & Cordoni, J.-P. 1981, A&A, 100, 307
Aurière, M., Le Fèvre, O., & Terzan, A. 1984, A&A, 138, 415
Baranne, A., Mayor, M., & Poncet, J. L. 1979, Vistas Astron., 23, 279
Bingham, E. A., Cacciari, C., Dickens, R. J., & Fusi Pecci, F. 1984, MNRAS, 209, 765
Buonanno, R., Corsi, C. E., & Fusi Pecci, F. 1985, A&A, 145, 97
Cudworth, K. M. 1976, AJ, 81, 519
Djorgovski, S., & King, I. R. 1986, ApJ, 305, L61
Dubath, P., Mayor, M., & Meylan, G. 1993, in ASP Conf. Ser., Vol. 50, Structure and Dynamics of Globular Clusters, ed. S. Djorgovski & G. Meylan (San Francisco: ASP), 69
Dubath, P., Meylan, G., & Mayor, M. 1990, A&A, 239, 142
———. 1994, A&A, submitted
Fahlman, G. G., & Richer, H. B. 1985, ApJS, 58, 225
Grabhorn, R. P., Cohn, H. N., Lugger, P. M., & Murphy, B. W. 1992, ApJ, 392, 86
Hartwick, F. D. A. 1970, ApJ, 161, 845
Hertz, P., & Grindlay, J. E. 1985, ApJ, 298, 95
Hesser, J. E., Harris, W. E., Vandenberg, D. A., Allwright, J. W. B., Shott, P., & Stetson P. B. 1987, PASP, 99, 739
Illingworth, G., & King, I. R. 1977, ApJ, 218, L109
Lauer, T. R., et al. 1991, ApJ, 369, L45
Mayor, M. 1980, A&A, 87, L1
Meylan, G., Dubath, P., & Mayor, M. 1991a, ApJ, 383, 587
———. 1991b, BAAS, 23, 833
Newell, B., & O'Neil, E. J. 1978, ApJS, 37, 27
Newell, B., Da Costa, G. S., & Norris, J. 1976, ApJ, 208, L55
Peterson, R. C., Seitzer, P., & Cudworth, K. M. 1989, ApJ, 347, 251
Phinney, E. S. 1993, MNRAS, in press
Phinney, E. S., & Sigurdsson, S. 1991, Nature, 349, 220
Racine, R., & McClure, R. D. 1989, PASP, 101, 731
Sandage, A., & Katem, B. 1977, ApJ, 215, 62
Sandage, A., Katem, B., & Kristian, J. 1968, ApJ, 153, L129
Stetson, P. B., & Harris, W. E. 1988, AJ, 96, 909
Zaggia, S., Capaccioli, M., & Piotto, G. 1992a, in Star Clusters and Stellar Evolution, ed. E. Brocato, F. Ferraro, & G. Piotto, Mem. Soc. Astron. Ital., 63, 211
Zaggia, S., Capaccioli, M., Piotto, G., & Stiavelli, M. 1992b, A&A, 258, 302
Zaggia, S., Capaccioli, M., & Piotto, G. 1993, A&A, 278, 475

Note added in proof.—In 1993 July, five high-resolution integrated-light echelle spectra of the core of M15 were obtained through a $1'' \times 8''$ slit, with exposures offset in $1''$ steps in order to cover a total central area of $5'' \times 8''$. The radial velocity and the velocity broadening of the cross-correlation function (CCF) were derived at all locations in this area by taking advantage of the spatial resolution along the slit. The velocity broadening of the CCFs is always ≤ 17 km s^{-1} at any location, i.e., we found no evidence for a velocity-dispersion cusp in the core of M15. In full agreement with the predictions of the present simulations, most of the CCFs are dominated by the light from one or two bright stars. This implies that any velocity dispersion estimate over an area of integration of the order of $1''$ square is affected by a very large statistical error. Over an area of $5'' \times 8''$, the statistical error is minimized by taking the average of all the *normalized* CCFs, which gives a velocity dispersion $\sigma_p = 11.7 \pm 2.6$ km s^{-1}. This value is consistent with the dispersion of the radial velocities of the 14 best resolved (spatially or spectroscopically) bright stars, determined from these new observations. Previous observational evidences of velocity dispersion cusp, streaming motion or core rotation, might be explained by two of the brightest central stars, separated by $2''.5$, which have radial velocities differing by 45.2 km s^{-1} (see Dubath, P., et al., Messenger, 74, 23 [1993]; Meylan, G., & Dubath, P., BAAS, 23, 1407 [1993]; Dubath, P., & Meylan, G., A&A, submitted [1994]).